energies

MDPI

Article

Practical Nonlinear Model Predictive Control for Improving Two-Wheel Vehicle Energy Consumption

Yesid Bello [1,2], Juan Sebastian Roncancio [1,2], Toufik Azib [1], Diego Patino [2], Cherif Larouci [1,*], Moussa Boukhnifer [3], Nassim Rizoug [1] and Fredy Ruiz [4]

[1] Energy and Embedded Systems for Transportation Research Department, ESTACA-LAB, 78066 Montigny-Le-Bretonneux, France
[2] Javeriana Electronics Department, Pontificia Universidad, Bogotá 110231, Colombia
[3] Université de Lorraine, LCOMS, F-57000 Metz, France
[4] Systems and Control Department Italy, Politecnico de Milano, 20158 Milan, Italy
* Correspondence: cherif.larouci@estaca.fr

Abstract: Increasing the range of electric vehicles (EVs) is possible with the help of eco-driving techniques, which are algorithms that consider internal and external factors, like performance limits and environmental conditions, such as weather. However, these constraints must include critical variables in energy consumption, such as driver preferences and external vehicle conditions. In this article, a reasonable energy-efficient non-linear model predictive control (NMPC) is built for an electric two-wheeler vehicle, considering the Paris-Brussels route with different driving profiles and driver preferences. Here, NMPC is successfully implemented in a test bed, showing how to obtain the different parameters of the optimization problem and the estimation of the energy for the closed-loop system from a practical point of view. The efficiency of the brushless DC motor (BLCD) is also included for this test bed. In addition, this document shows that the proposal increases the chance of traveling the given route with a distance accuracy of approximately 1.5% while simultaneously boosting the vehicle autonomy by almost 20%. The practical result indicates that the strategy based on an NMPC algorithm can significantly boost the driver's chance of completing the journey. If the vehicle energy is insufficient to succeed in the trip, the algorithm can guide the minimal State of Charge (SOC) required to complete the journey to reduce the driver energy-related uncertainty to a minimum.

Keywords: NMPC; two wheel; electric vehicle; eco-driving profile; efficiency; optimization; autonomy increasing

Citation: Bello, Y.; Roncancio, J.S.; Azib, T.; Patino, D.; Larouci, C.; Boukhnifer, M.; Rizoug, N.; Ruiz, F. Practical Nonlinear Model Predictive Control for Improving Two-Wheel Vehicle Energy Consumption. *Energies* **2023**, *16*, 1950. https://doi.org/10.3390/en16041950

Academic Editor: Mojtaba Ahmadieh Khanesar

Received: 5 December 2022
Revised: 23 January 2023
Accepted: 6 February 2023
Published: 15 February 2023

1. Introduction

Technology is improving the efficiency and use of electric automobiles due to the increasing number of electric vehicles (EVs) on the market. EVs are becoming increasingly popular since they are considered a clean option in terms of pollution, even though they face various challenges (charging time, range, standardization of the charging process, charging stations, and the recycling process). The balance between an eco-driving profile and performance impacts the autonomy of the electric vehicle. EVs can be charged heavily using renewable energy systems, which means fewer carbon emissions and more use of renewable energy [1]. Switching to EVs can help reduce greenhouse gas emissions and help people in some countries get ahead economically.

Advanced Driver Assistance Systems (ADAS) are algorithms that assist the driver. According to [2,3], the algorithm's main task is to set performance boundaries for a vehicle based on a given criterion. Theoretical models, historical data, or unsupervised learning systems can all be used [4–6]. When the algorithm determines that the current power demand is insufficient to complete the journey, constraints on the use of the driver modes are placed on the vehicle's performance [5]. These settings can be divided into Eco, Normal,

and Sports categories. The constraints may change depending on the algorithm. In some cases, it alludes to the maximum motor power, maximum acceleration, or top speed [7,8]. There are also cases when eco-driving is computed when receiving trip time importance and presenting each road point's optimal speed [9].

Several techniques can improve the driving profile and vehicle-based autonomy [10]. The two most common are the driving alert system and the eco-driving characteristics optimizer [11]. The distinction between them is the assessment of energy needs. The driving alert system is used to notify the driver if the energy available in the vehicle is insufficient to continue the trip. In the eco-driving optimizer, energy estimation helps to decide what type of driving mode is necessary to ensure an energy consumption rate for the duration of the trip. Therefore, the bounds provided by the speed profile optimizer are constant and, in some cases, excessive concerning the actual needs of the driver. In particular weather and road conditions, the efficiency of the BLDC engine decreases from 64% to 12%. Moreover, it has been proven that the input parameters affect an electric motorcycle's dynamic characteristics and consumption characteristics [12].

In this study, evaluating autonomy involves using dynamic models and external data to ascertain whether the driver can successfully achieve the route. Considering factors such as traffic, vehicle limits, and driver preferences can determine the ideal speed profile to lower total energy use. Therefore, an eco-driving approach using a non-linear predictive controller has been developed. All-electric vehicles can use the eco-driving strategy. However, this article concentrates on two-wheeled EVs because the driver's activities account for the majority of energy consumption, and the size of the vehicles imposes additional limits that must be taken into account. In [12], a simulation model of the electric motorcycle was used to determine the velocity, propulsion torque, and electric consumption characteristics with variable electric motorcycle mass, driver mass, wheel radius, frontal area, and transmission ratio.

In this article, eco-driving algorithm design incorporates thermal, electrical, mechanical, and theoretical models to predict power usage. To do that, the non-linear model predictive controller (NMPC) is a helpful technique for prediction and optimization, for example, in speed terms, [13]. This work develops a tool that enables users to maximize energy efficiency depending on input data such as state of charge (SOC), distance traveled, elapsed time, and speed. Because of this procedure, the EV will tell the driver the best speed and driving conditions to cover the remaining distance most efficiently and cost-effectively. This research shows how to implement the NMPC and practically compute different optimization problem parameters, such as (i) Weights of the cost function, (ii) Necessary physical bounds in the constraints, and (iii) Efficiency of the motor concerning torque and speed. This article gives a deeper understanding of what the authors proposed in [14] and presents experimental results through a testbed platform. Here, it is shown how the test bed is built and adapted to emulate the route Paris-Brussels. Practical implementation in the test bed is crucial since it validates results from theory. Results indicate that the strategy based on an MPC algorithm can significantly boost the driver's chance of completing the journey. If the vehicle's energy is insufficient to succeed in the trip, the algorithm can guide the minimal State of Charge (SOC) required to complete the journey to reduce the driver's energy-related uncertainty to a minimum. It gives results that can be achieved afterward to integrate different power sources [15].

The rest of the paper is organized as follows. Section 2 presents the mathematical model used in this work. Section 3 explains the closed-loop controller considering perturbations. The experimental platform development that served as the basis for the present research can be detailed in Section 4. The model validation is presented in Section 5, and the experimental results and some findings of this research are presented in Section 6. Finally, conclusions and future studies are given in Section 7.

2. Mathematical Model

This section summarizes the mechanical model used to represent the degrees of freedom of the vehicle motion. All the variables are listed at the beginning of this article. The longitudinal model examines the accumulation of forces along the X-axis. Longitudinal dynamics are set as shown in Figure 1. Other phenomena, such as wheel slip and angular velocity, are excluded from this study [16–18]. According to [16], Newton's second law of motion in the X-axis is stated in Equation (1).

$$m\ddot{x} = \frac{T}{R_{wf}} + F_{roll} + F_{aer_x} + F_w sin(\theta_s) sin(\beta) \tag{1}$$

Considering that the aerodynamic force, rolling resistance force, and road slope are all critical forces in a vehicle's longitudinal motion [19,20], the aerodynamic force and Rolling Resistance Force are stated as in (2) and (3), respectively.

$$F_{aer} = \frac{-1}{2} \rho C_d A_f (V_{wind} * cos(\alpha_{air}))^2 \tag{2}$$

$$F_{roll} = -(\mu_0 + \mu_1 \dot{x}^2) F_z cos(\theta_s) \tag{3}$$

Road friction parameters can take values from 0.001 to 0.00082 according to the road conditions (new, wet, frozen, etc.) [20]. β is assumed used to be near 90°. Road Slope is stated as $F_w = mg$. The total traction force, from the right-hand of Equation (1), is computed based on a power profile associated with θ_s. This process is vital for comparing the performance of different vehicles since the energy demand depends indirectly on speed values and the energy required by the EV to maintain a desired speed, for example, if there are considered different road classifications (urban or rural), climate, and driving skills can also be included in driving profiles.

The driving profile is the representation of vehicle speed vs. time. The shapes are advantageous to designing, calibrating, or improving the test. Different driving cycles exist, such as (EPA - United States Environmental Protection Agency, WLTP, and NEDC—created by UNECE World Forum for Harmonization of Vehicle Regulations, Artemis—cycles created during the Artemis project in EU) [21]. Figure 2 shows six different driving profiles, which is helpful for the research.

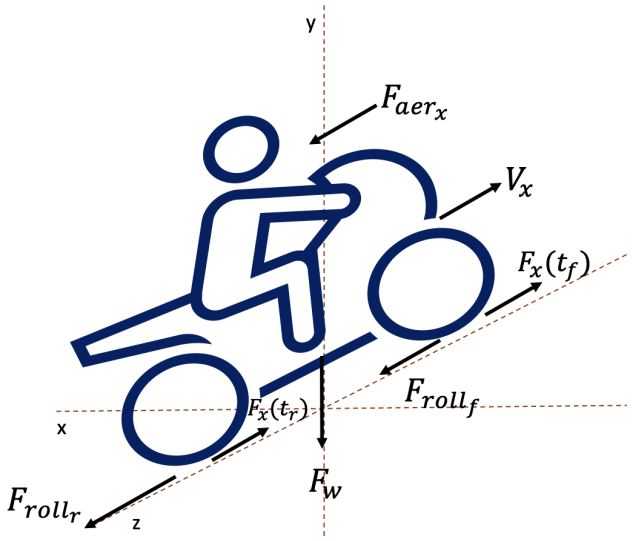

Figure 1. Force Diagram.

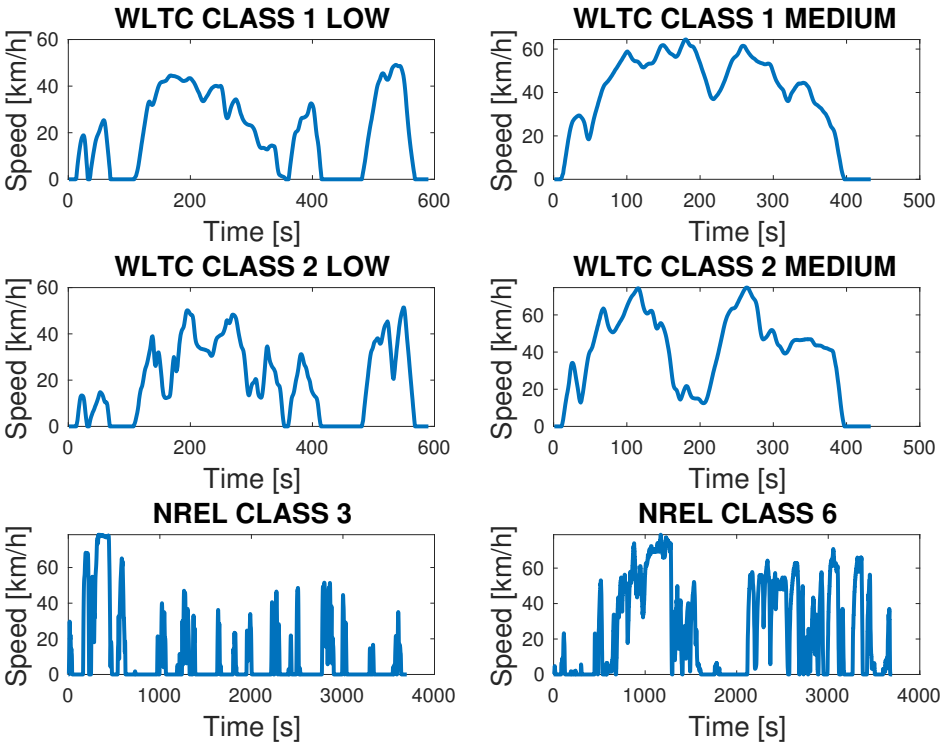

Figure 2. Driving Cycles for Evaluation.

Therefore, the energy used is a function of how a vehicle of 150 kg is affected by outside forces and how well it works electrically. The study's target route is Paris to Brussels, and Google Maps determines the slope profile and wind speed data. Its analysis is required to improve the performance of the controller. Moreover, according to [22], energy losses may exist in various electrical or mechanical devices. Indeed, power losses are caused by the BLDC motor's electrical and magnetic properties. Magnetic losses are caused by temperature fluctuations in the motor's magnetic material. There are also losses which are due to power loss in the winding. When the winding is loaded, core losses result from the unintended magnetization of the core via inductive action [23–26].

Consequently, an efficiency map's geometric representation can orient the optimal controller in the correct direction and reduce the energy estimation error [18,27]. In [14], a "Cauer network" is proposed in each circumstance to alter the resistance and capacitance values anticipated by electrical models under temperature changes. The battery losses are incorporated into the model, allowing for consideration of the internal losses of the battery and their temperature-dependent change. Then, the expected error in energy use can be kept below 5% without making the electrical models challenging to understand [28,29]. Therefore, according to [14], energy E can be modeled as stated in (4).

$$\dot{E} = \frac{T}{R_{wf} Eff(\dot{x}, T)} \dot{x} \tag{4}$$

where $Eff(\dot{x}, T)$ represents the geometrical abstraction of the motor efficiency that shows how the vehicle can behave in the real world [14].

3. Model Predictive Control

This section shows a proposal for a Non-linear model predictive control (NMPC). Its objective is to determine the proper torque T to drive a given distance using the least feasible energy. Figure 3 depicts the implemented controller. It has a prediction horizon of $N = 10$. These values balance the compilation time and speed/acceleration dynamics.

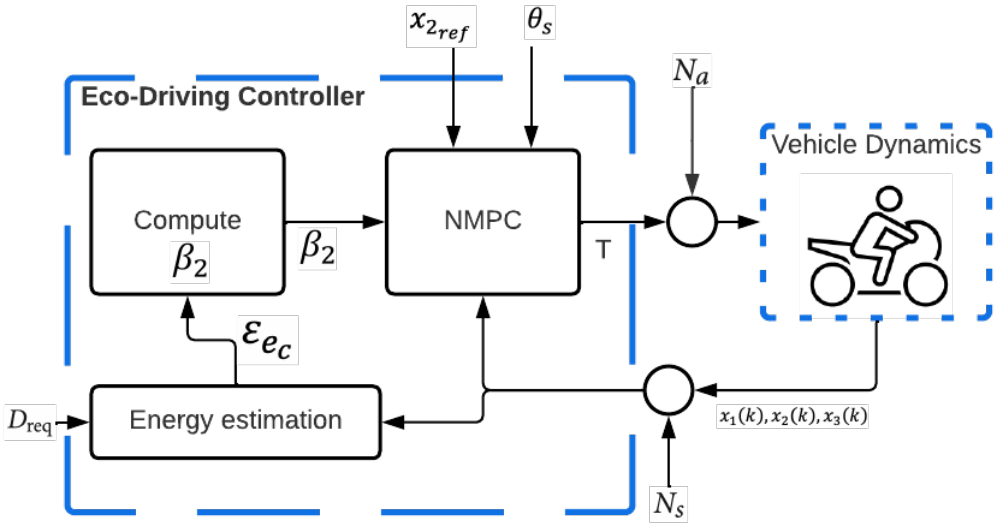

Figure 3. Control Diagram.

The proposed controller Figure 3 calculates the energy required to finish the trip ε_{e_c} based on the remaining distance traveled D_{req} and the current vehicle dynamics. External variables related to noise from the N_a actuators and N_s sensors are also included in the control loop. The vehicle's driver determines the speed $x_{2_{ref}}$. However, based on the driver's behavior and the estimated energy path, the system suggests the optimal driving style β_2 to be adopted by the driver. The algorithm implemented by the NMPC controller is shown in Figure 4. There are both external and internal sources of errors. External factors, such as traffic signals, influence the behavior of a vehicle driver. Internal sources include sensors and actuators and can also alter the operation depending on their performance. The closed-loop controller must also be able to reduce the impact of disturbances on vehicle energy performance.

The estimated speed profile is responsive to the driver's desires but bounds the maximum speed values and tends to bring the average speed closer to the most efficient speed value based on the torque required. The optimal problem solved by the NMPC is stated in Equations (5)–(11).

$$\min \quad J(x,\ T,\ k) \tag{5}$$

$$J(x,T,k) = \beta_1\beta_2\phi_1(x_3(N)) + \sum_{0}^{N} -\beta_2\phi_2(x_2(k),T(k)) + (x_2(k) - x_{2_{ref}})^2 \tag{6}$$

$$\text{s.t.} \quad T_{min} \leq T(k) \leq T_{max} \tag{7}$$

$$0 \leq x_1(k) \leq x_{1_f} \tag{8}$$

$$x_{2_{min}} \leq x_2(k) \leq x_{2_{max}} \tag{9}$$

$$0 \leq x_3(k) \leq TotEne \tag{10}$$

$$x(k+1) = f(x(k),\ T) \tag{11}$$

where (5) and (6) represent the objective function of the NMPC, β_1 and β_2 are parameters for the optimization problem. β_2 is computed to be used within the forecast horizon without exceeding the vehicle or system capabilities and the estimation of the energy to finish the journey ε_{e_c} [14]. Constraint (7) is the physical constraint that describes the maximum force mechanical structures can generate, including the maximum torque the system can produce. The vehicle cannot replicate the behavior if the states are outside this feasible region. Constraints (8) and (9) impose the feasible region and avoid an over-damped behavior; constraint (10) is a physical limitation of the quantity of energy available in the battery. (4), $x(k)$ is a vector composed by the discrete variable of x, $\dot{x}$ and E. Finally, ϕ_1 to

ϕ_2 are stated in (12) and (13) and (11) is a simplified discrete representation of the model given in (1).

$$\phi_1\left(x_3(k)\right) = x_3(k) \tag{12}$$

$$\phi_2\left(x_2(k), T(k)\right) = Eff(x_2, T) \tag{13}$$

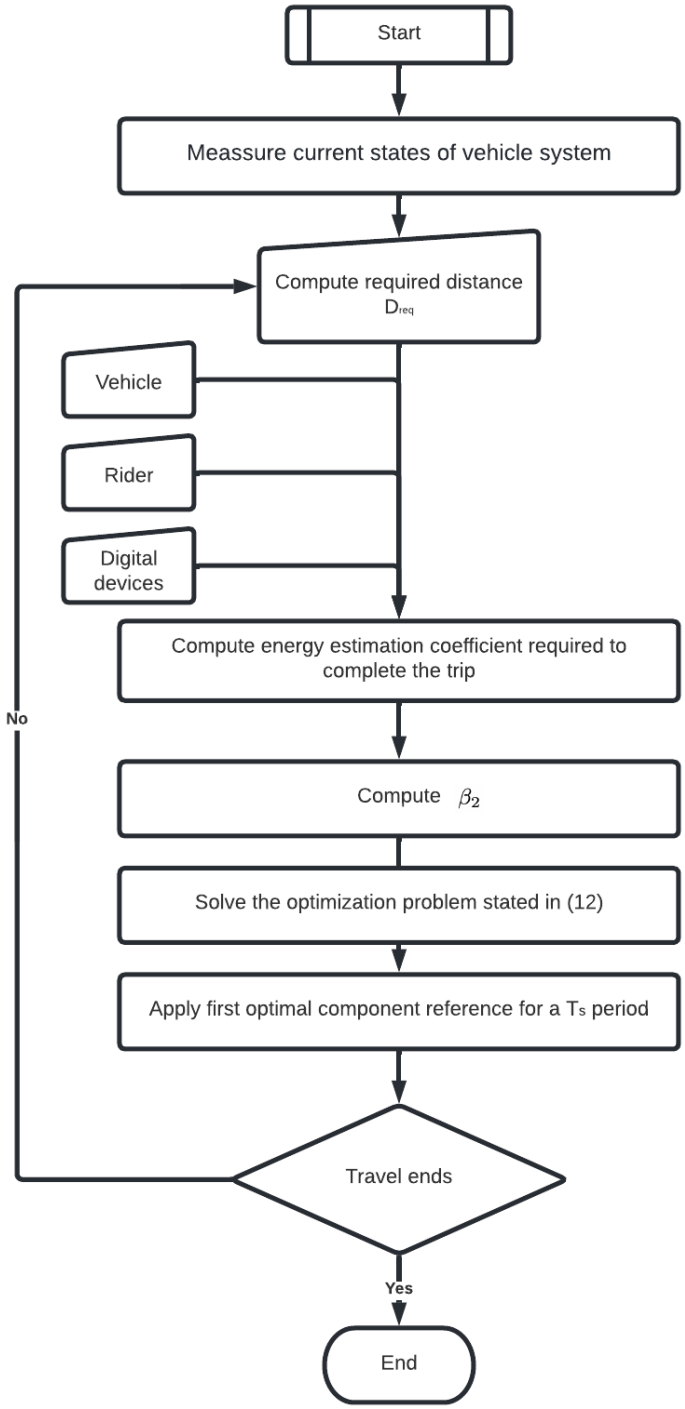

Figure 4. NMPC Algorithm.

4. Experimental Platform

One of the objectives of this research is to propose a viable method for estimating efficiency values in real-time of EV. In addition, it is necessary to ensure the accuracy of the estimation process in the control algorithm. For achieving accuracy and viability, a scale motorcycle model is built with a test bench to validate the proposed method (see Figure 5). Furthermore, the geometric representation can be modified depending on the engine parameters to obtain any efficiency point from the hyperbolic Equation (14). In the test, two main characteristics are altered. First, the engine power is decreased due to safety constraints, and the speed profile used is WLTP in urban, rural, and mixed environments. Thus, this section describes the mechanical specifications of the motorcycle platform and the framework required to reflect internal and external events during operation accurately. Experiments are conducted to determine the controller parameters indicated in the previous section.

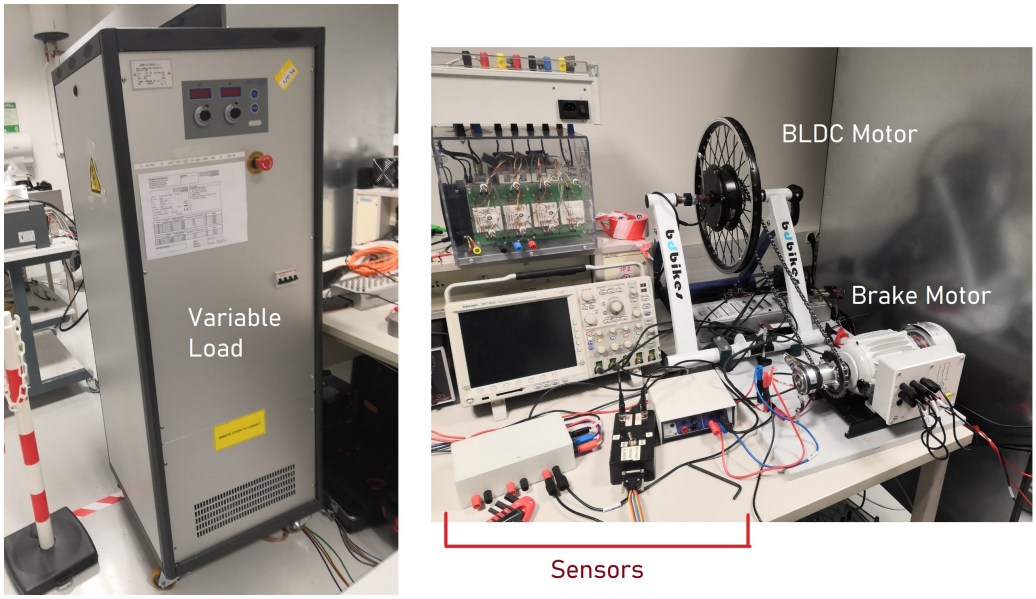

Figure 5. Practical Test bench image.

4.1. Specifications

The test bench consists of a BLDC motor that replicates the motorcycle's traction (traction motor). The traction motor is supported by a framework that ensures its integrity even at maximum torque and speed. In addition, a system that may be adjusted to define several torque profiles due to wind, slope, or weight variations is incorporated. In this method, opposing forces are simulated by a torque generator by a 300-Watt auxiliary engine connected to the traction motor through a generator-equipped bicycle chain. Both electric machineries (traction motor and generator) are coupled to a 32-toothed cycling disc. A Zenon load AL3008BLDC-200V-10KW MD2-1.06 is used to change the torque of the generator. The Semikron 08753450/309 inverter interacts with the generator and the load. This component rectifies the current profile of the asynchronous motor to supply the changeable load with the current. Figure 5 depicts the experimental setup.

A BLDC1200 W from the OZO Speed Donkey kit with a maximum power rating of 1200 W, rated at 1000 W, and bounded to 25 A, is used. This kit converts conventional motorcycles to electricity, and the maximum torque is 98 Nm and the maximum top speed is 30 km/h (due to the power supply of 36 V). It includes a field-oriented control mechanism (FOC) and the option to contain or exclude Hall effect sensors. Here, dSPACE DS1104 real-time controller board is the hardware and software interface. The traction is measured using the encoder XCC1514TSM02Y with a constraint of 6000 rpm as the maximum revolution speed. Figure 6 shows the electric integration between different elements.

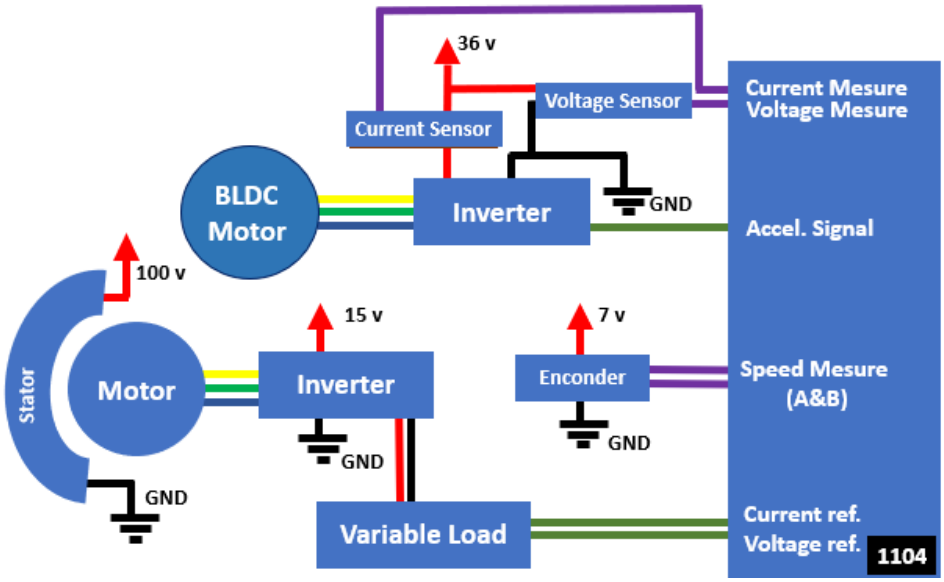

Figure 6. Electrical diagram of the test bench.

In determining the relationship between the voltage of the throttle signal and the speed of the traction motor, the signal range is determined, and the throttle signal and traction motor speed are compared. The measured voltage range for the unaltered throttle signal is between 1.35 V and 2.65 V. This value means that the traction motor speed can be controlled with a V_{ref} from 0 to 12 m/s. This values determines v_{min} and v_{max}. The equation which describes the data behavior is $V_{ac} = V_{ref} * (1/9.23) + (12.4/9.23)$, where V_{ac} and V_{ref} are the acceleration in volts and velocity in meters per second, the behavior is showed in Figure 7.

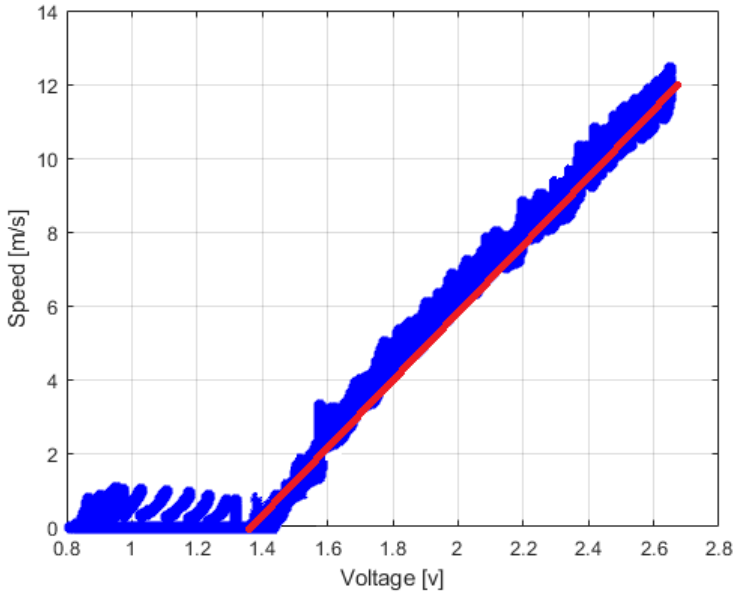

Figure 7. Accelerator vs. motor speed voltage behavior.

It is important to consider noise due to hardware and software components. There are two significant noise sources, the interaction between the sensor and the analog-to-digital converter on the DSpace board and the exchange between the actuator and the digital-to-analog converter. Furthermore, they can produce system oscillation.

The characteristics of the test are shown in Table 1 and in [30]. The sensors have errors of 0.12 and 0.02, respectively. Moreover, the actuator error resulting from throttle and driver

variations has an RMS error of 0.4, which is incorporated into the ADC resolution, which can affect the open loop motor controllability is essential.

Table 1. Parameters related to Test bed [30].

Device	Parameter	Value
Motor System	Technology	BLDC
	Nominal power	1200 [W]
	Max power	1365 [W]
	Max speed	40 [km/h]
	Max torque	98 [Nm]
	Wheel diameter	21 [cm]
Braking System	Technology	Brushless
	Nominal power	300 [W]
	Max current	0.95 [A]
	Max speed	1500 [rpm]
BLDC inverter	Control technique	full wave rectifier
	Nominal voltage	15 [V]
	Max voltage	56 [V]
	Max output current	25 [A]
Brake inverter	Control technique	Full wave rectifier
	Nominal control voltage	15 [V]
	Nominal voltage	200 [V]
	Max output current	25 [A]
Encoder	Encoder type	Incremental encoder
	Shaft diameter	14 [mm]
	Resolution	256 to 4096 [points]
	Max speed	60,006 [rpm]
	Voltage Supply	5 to 30 [V]- DC
Voltage sensor	Range	500 [V]
	Resolution	100 [mV]
	Voltage Supply	220–240 [V]-AC
Current sensor	Range	50 [A]
	Resolution	10 [mA]
	Supply voltage	220–240 [V] - AC
Variable load	Voltage range	10–1000 [V]
	Voltage resolution	100 [mV]
	Max input power	14 [kW]
	Current resolution	100 [mA]
	Voltage Supply	220–240 [V] tri phases
DSpace card	I/O range	−10 to 10 [V]
	I/O resolution	1 [mV]
	I/O max current	0.005 [A]
	Voltage Supply	12 [V]

Speed profile NREL class 3 described in Section 2 gives the least sensitive energy behavior for external perturbations, with a 16% increase over the projected energy per kilometer. In addition, the WLTC class 2 velocity profile is most influenced by disturbances present on the experimental platform, with an increase in power per kilometer of 25%.

4.2. Efficiency and Bounds

The mechanical limits and efficiency maps were derived by logical programming, co-simulation, and the magnetic simulation software ANSYS/Maxwell©), such as in [31]. The assessed parameters of the electric motor are shown in Table 1 as in [30]. This initial stage allows the estimation of subsequent phases' and predicts outcomes.

Then, perform rotor blocking testing. This test attempts to impede the rotor with a progressive load. Throughout each trial, the load must exceed the motor's maximum load at maximum speed. Consequently, the rotor's speed must decrease, and the mechanical limits of the engine will be identified. This process is crucial to prevent motor damage and to remember that the maximum torque obtained during this test must be less than 90 percent of the maximum torque motor limitation. Next, the values of the efficiency maps inside the area identified by the rotor blockage test were calculated. The data are extracted from the datasheet, and the traction motor parameters are shown in Table 1. Then, construct a linear representation of the mechanical motor restrictions determined in the preceding phase. Finally, Check the maximum efficiency level. Since an initial efficiency estimate is made in step 1, verifying the maximum value by working as near as feasible to that point and measuring the efficiency value is necessary. After the co-simulation process shown in Figure 8, the rotor blocking test gradually obstructs the motor's rotor. In addition, because torque cannot be measured, the link between speed and torque shown in the depiction of simulated efficiency is used. A method for preventing exceeding 90 percent of the maximum torque is keeping the speed value at no less than 30 percent of the maximum speed. From Figure 8, it is around 160 rpm.

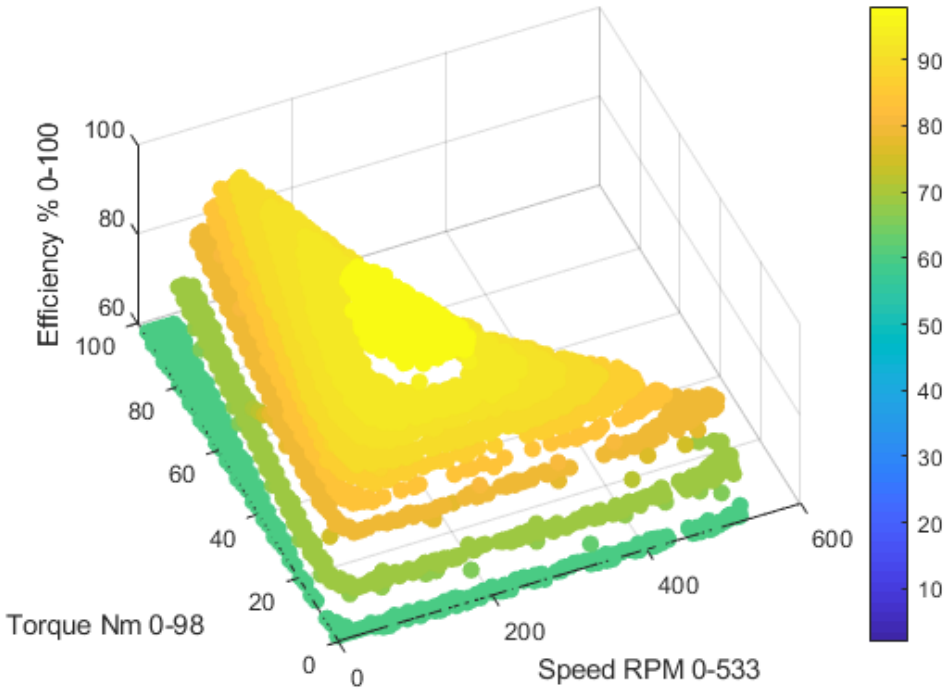

Figure 8. Efficiency map estimation result $Eff(x_2, T)$.

Due to the rotor blocking test, the speed restriction shown in Figure 9 is determined. This representation is oriented and positioned again in a plane (speed-torque) using the following information: minimum and maximum speed ($x_{2_{min}} = 0$ and $x_{2_{max}} = 12$), minimal

and maximal torque ($T_{min} = 0$ and $T_{max} = 95$), and co-simulation results as shown in Figure 10.

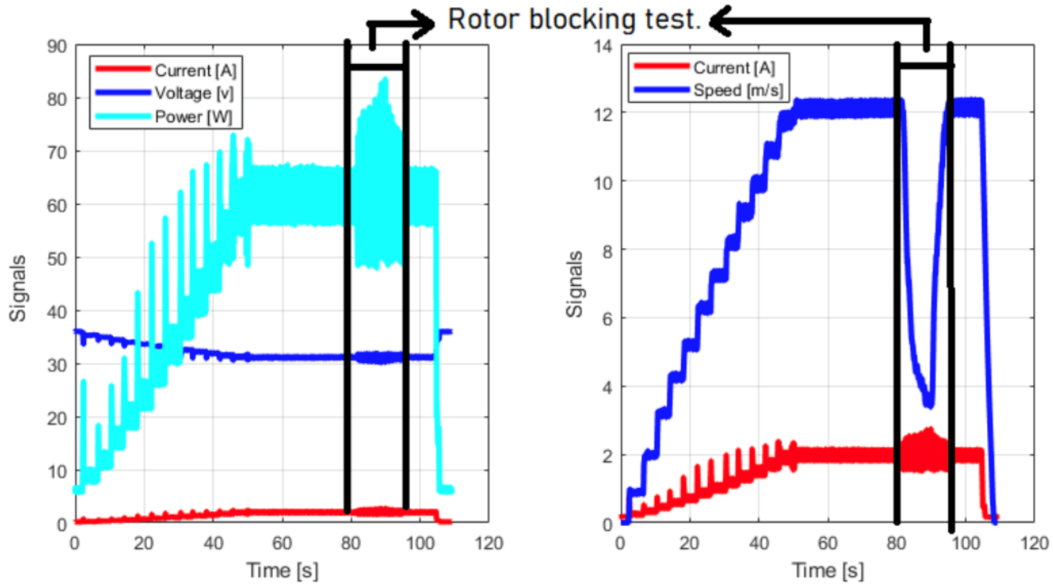

Figure 9. Experimental result of speed curve during rotor blocking test.

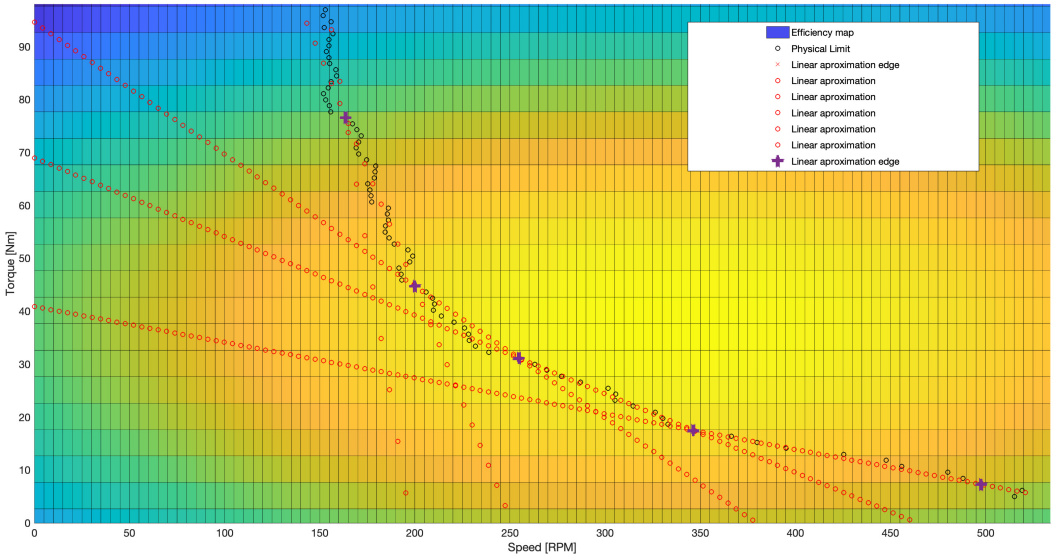

Figure 10. Simplified efficiency representation.

After obtaining the constraint speed curve, linear representations are incorporated and integrated into the estimation process. The linear expressions defined by the expression: $Y_i = m_i X_i + b_i$. Where Y_i is the torque, i_{st} X_i is the velocity i-st, and b_i, m_i are the Y-axis intercept and the slope. The obtained values are presented in Table 2, which shows the linear representations of the physical limits of the system. It is essential to mention that this approximation is made to avoid the overburden in computation time due to nonlinearity. Figure 10 shows the speed-torque constraints of the motor with the efficiency map and the linear approximations with the points where these limits start and end.

Finally, the geometrical representation needs a suitable efficiency value to orient the optimization issue from NMPC in Equations (5)–(11). To verify convergence, the bike training roller's brake is used to measure torque near maximal efficiency. Zenon variable electrical load makes modest modifications. The geometrical representation's proposed total efficiency point is inaccurate by 67 rpm in speed and 7.1 Nm in torque. The Speed-

Torque limitations curve and simulated efficiency map from Figure 8 are used to calibrate this number. Thus, the geometrical representation shifts to the maximum point. The simulation and calibration resulted in Figure 10 and Equation (14).

$$Eff(T, x_2) = B_0 - B_1(T - x_c)^2 - B_2(x_2 - y_c)^2 \quad (14)$$

where $B_0 = 92.6$, $B_1 = 1.2859e^{-4}$, $B_2 = 0.0011$, $x_c = 204$ and $y_c = 32.6$.

Table 2. Linear approximation of torque-speed constraints.

Slope	Value	Intercept	Value
m_1	−2.92	b_1	40.86
m_2	−6.45	b_2	68.96
m_3	−10.81	b_3	94.57
m_4	−37.97	b_4	219.74
m_5	−97.18	b_5	443.03

Figure 10 represents the physical constraints of the experiment. The absolute power limits of the torque speed curve, which has a non-linear nature, are depicted in black "o". Because of the non-linear limitations, an approximation to the natural limits is required; the approximation is replicated by the five red "o" curves. This recreation aims to develop a series of linear functions "function by parts" to linearize the physical limits to ensure the shortest possible computation time in the MPC structure. Each linear limit's change limits are denoted by an "x" in red.

4.3. Speed and Energy Coefficient

Once the efficiency function has been computed, the information must be included in the block "energy estimation" of Figure 3. This parameter allows you to evaluate the battery's energy quantity concerning the required distance to perform a more stringent or light estimation. The first test estimates the energy parameter along the velocity signal in the form of steps. This test allows investigation of the energy coefficient at various values to check the suggested efficiency function and demonstrate the minimal energy coefficient the controller platform can get in constant speed profiles. The current, velocity, power, and voltage signals are displayed in Figure 11 are acquired due to the test.

The power is integrated along the time corresponding to each step and divided by the distance covered to calculate the energy used in each speed signal phase in stairs shapes. Torque area test from 0 to 10 Nm is also essential. This torque spans all speeds. The driver's necessary distance and battery SOC are used to calculate the highest practicable energy coefficient needed to complete the journey. The ε_{e_c} coefficient is determined from the total energy consumed over the trip's distance and represents the energy used per kilometer. In addition, the estimation block looks at past traffic data to estimate the speed profile. Estimating the profile is vital for the Eco-Driving Controller to work in real-time and to take into account the randomness of the actual driving cycle. Figure 12 depicts the relationship between EFF and β_2. In this figure, while the β_2 increases, the energy required to achieve the trip decreases. Figure 12 shows the energy coefficient data and the ε_{e_c} energy estimation comparison with β_2.

Now that the whole efficiency function and parameters have been calculated, a test to achieve the β_2 value may be performed. This test estimates the speed profile along various variables to determine the controller's optimal performance. This test is performed without any extra disturbance (actuator and sensor disturbances proper of test bed), and the velocity profile estimates are assured of avoiding a perturbation that an open-loop controller cannot fix. As a result of the tests, the most efficient velocity in this torque range is roughly 4 m/s, which translates to 204.6 rpm. Then, increasing β_2 always ensures that the energy coefficient goes down. Lastly, Figure 12 shows the result of this test.

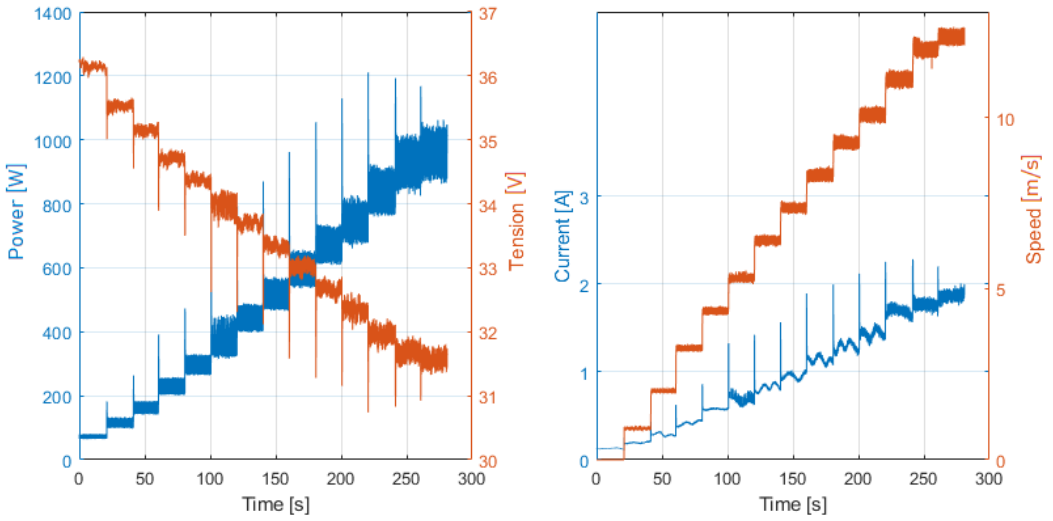

Figure 11. Speed vs. Power.

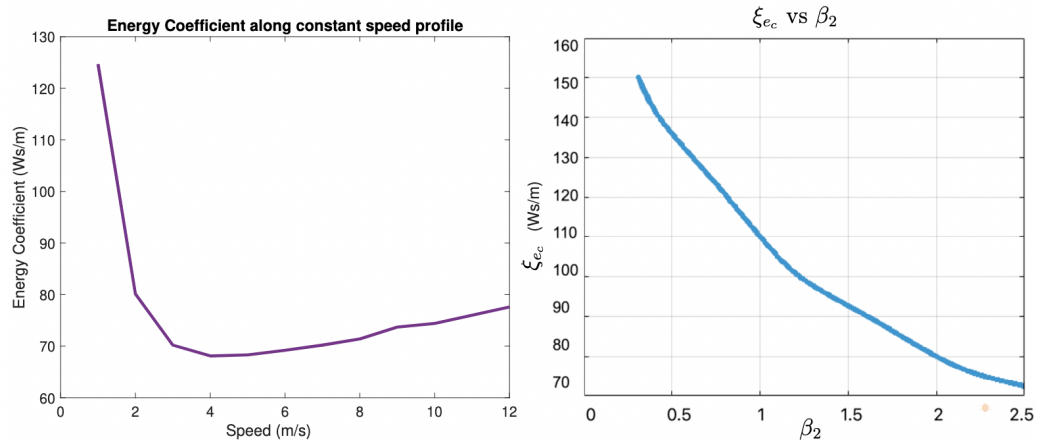

Figure 12. Energy coefficient behavior.

5. Model Validation

The approach used to validate the mathematical model with the experimental model under specific operation settings is described in the following paragraphs. In this section, it is vital to note that, according to [17], lateral dynamics are not required to indicate the vehicle's energy condition. This assumption is only valid if the speed is less than 60 km/h, and as demonstrated below, all tests are only valid for velocities less than 60 km/h; indeed, the testbed has a max speed of 40 km/h. The proposed road (see Figure 13) consists of two 50-meter-radius curves with a bank angle of 30% and a junction with an elevation of 2 meters and a slope angle of 5°. A virtual test scenario is incorporated into a vehicle dynamic simulation tool to validate the model's behavior. Two tests are conducted: one with constant and varying speeds to determine the yaw reaction at different speeds and another with variable speeds within the same range to determine the error's dynamic response.

Figure 13. Designed Road.

5.1. Constant Speed Test

This test verifies the behavior shown in Equation (1) and identifies discrepancies in the model. Using the linear pneumatic friction model, the inaccuracy of angle yaw increases rapidly. As shown in Figure 14, the estimation is deemed acceptable if the longitudinal and lateral speed has an error less than 5%.

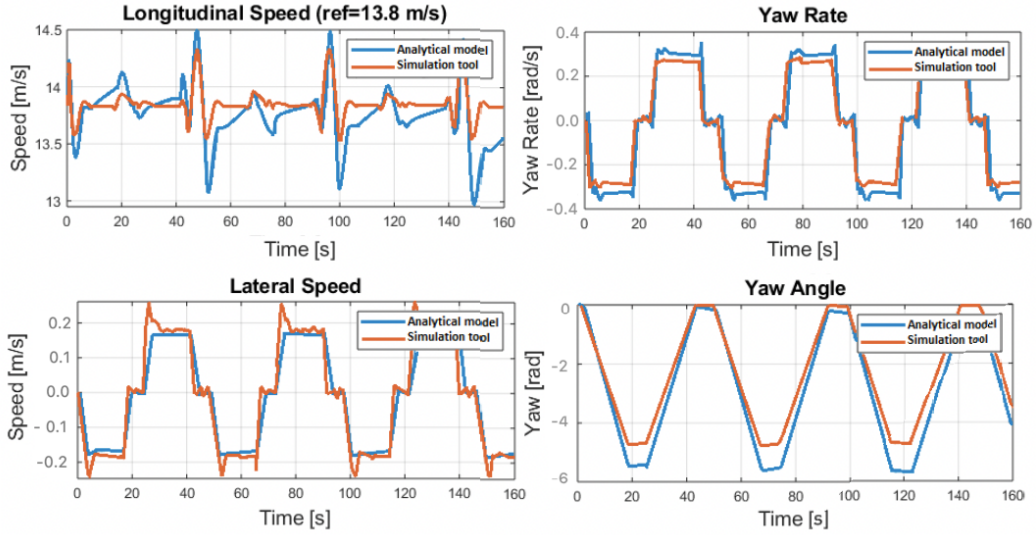

Figure 14. Static speed profile results (error percentage).

Therefore, a speed profile estimator cannot use yaw information as a constraint under these conditions. Figure 15 displays the test's error rate.

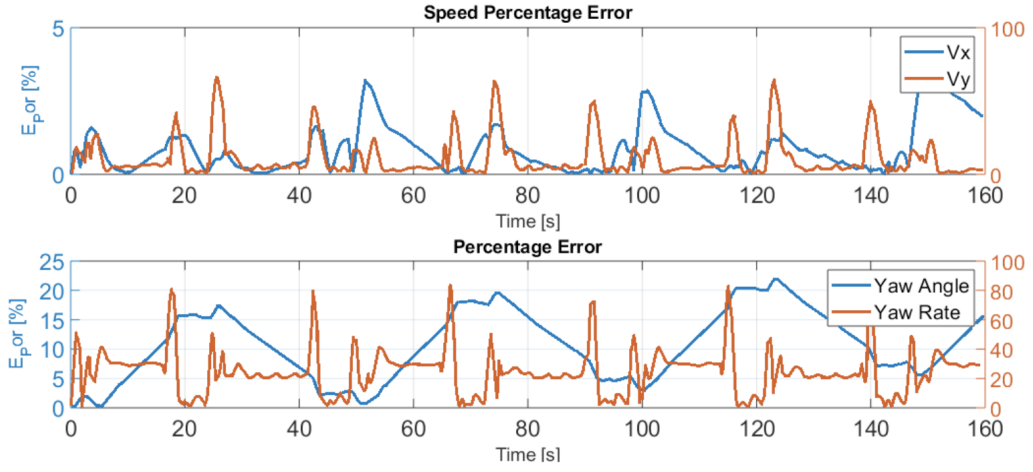

Figure 15. Static speed profile results (error percentage).

5.2. Dynamic Speed Test

Due to changing speed references, this test's error rate may rise. As illustrated in Figure 16, under dynamic speed conditions, a forecast horizon of fewer than 10 s is reasonable.

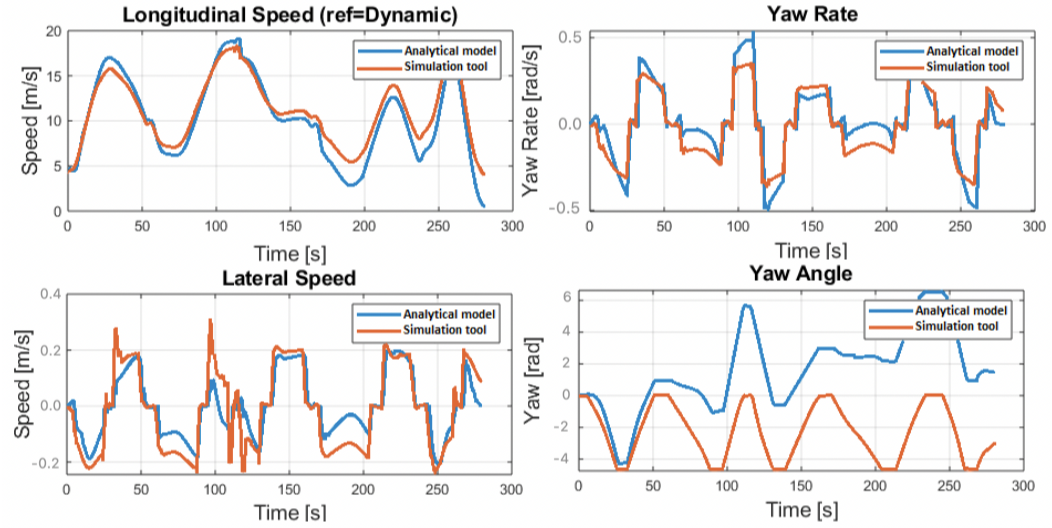

Figure 16. Dynamic speed profile results (error percentage).

Figure 17 depicts the prediction horizon for the model's present accuracy. These results demonstrate the prediction horizon in 8 s for errors in longitudinal velocity and yaw angle of less than 10%.

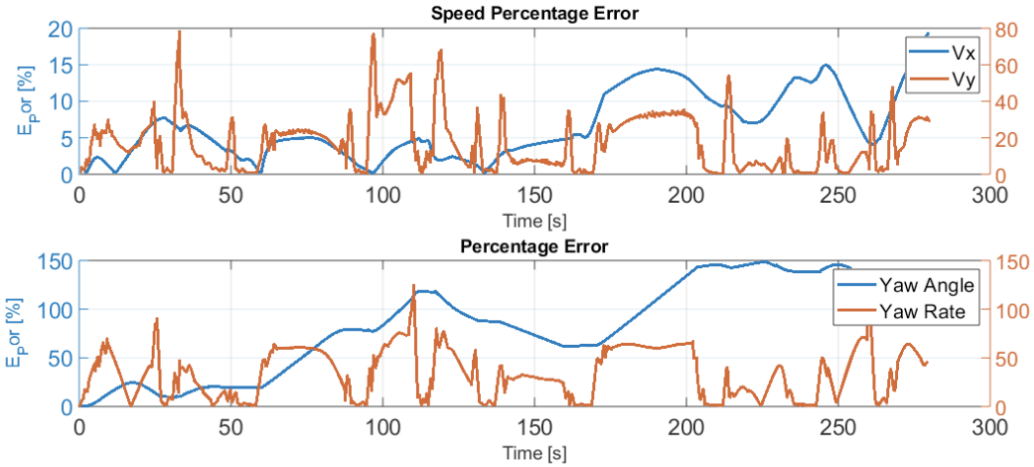

Figure 17. Dynamic speed profile results (error percentage).

To fully understand the impact of the current findings, a sensitivity analysis must be conducted to see how the error % varies as a function of the friction coefficients. However, the Pacejka equation represents the friction coefficients' non-linear behavior in the simulator, despite the model's assumption that they are constant. (see Figure 18 [17]), better results are expected with a more accurate estimation of these parameters for a 0 to 60 km/h urban drive profile.

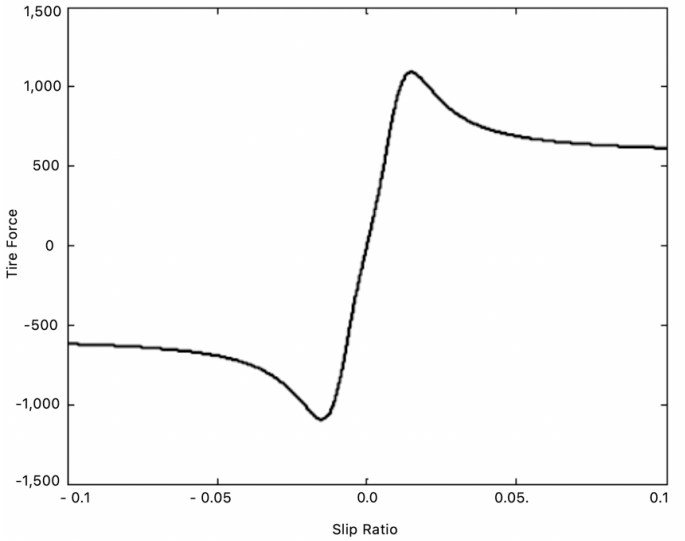

Figure 18. Tire Pressure Curve Calculator (with Magical Formula- Pacejka equation).

5.3. Simulation Results after Sensitivity Test

The sensitivity test is based on how each adjustment in friction coefficient impacts the average percentage error between the analytical model and the simulated model. The pneumatics industry has recognized physical limits to pneumatic dynamics and friction coefficients, which are described by minimum and maximum test results. It is crucial to note that in the test with an a priori estimation value, only one of the four parameters changes during the experiment. The selected delta values guarantee that the model's state does not fluctuate by more than half a percent from iteration to iteration. The average yaw error fell by 73% after new friction coefficients were implemented, as expected by the sensitivity analysis. According to the results of the static speed test (shown in Figures 19 and 20, the average error percentage is 1.15 percent for longitudinal speed and 3.40 percent for yaw angle. Even if the mean errors increase during the test, the ratio stays around 1/100 s for a longitudinal speed and 1/40 s for a yaw angle.

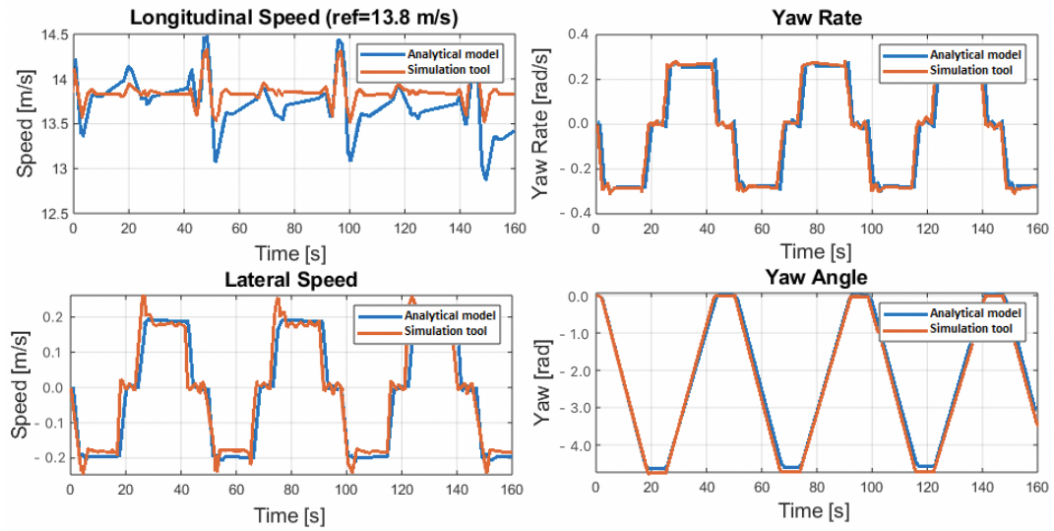

Figure 19. Static speed profile results after sensitivity test.

Moreover, the dynamic speed test in Figures 21 and 22 indicate a mean error percentage of 4.47% for longitudinal speed and 23.12% for yaw angle, with the sensitivity changes. The revised friction coefficients determined by the sensitivity test drop to 71.97% of the

mean error percentage during the dynamic speed test compared to the previously reported yaw mean error percentage.

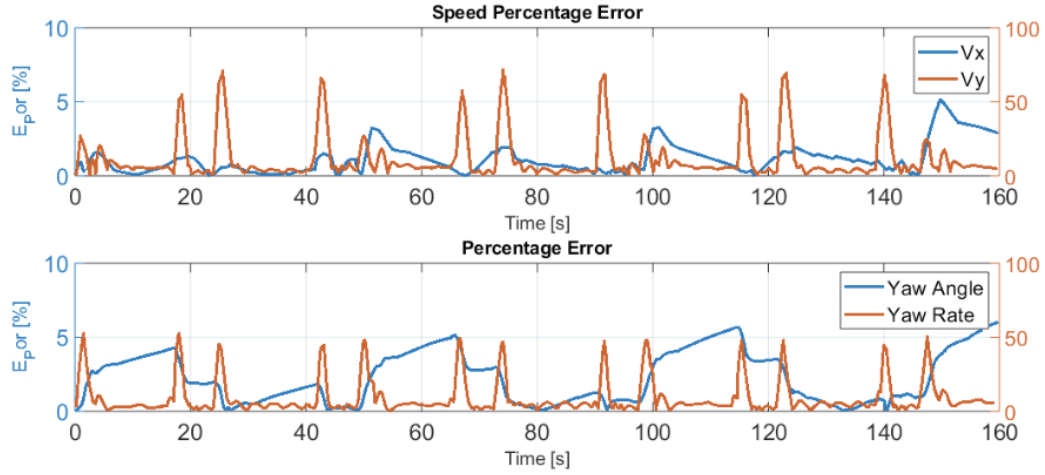

Figure 20. Static speed profile results after sensitivity test (error percentage).

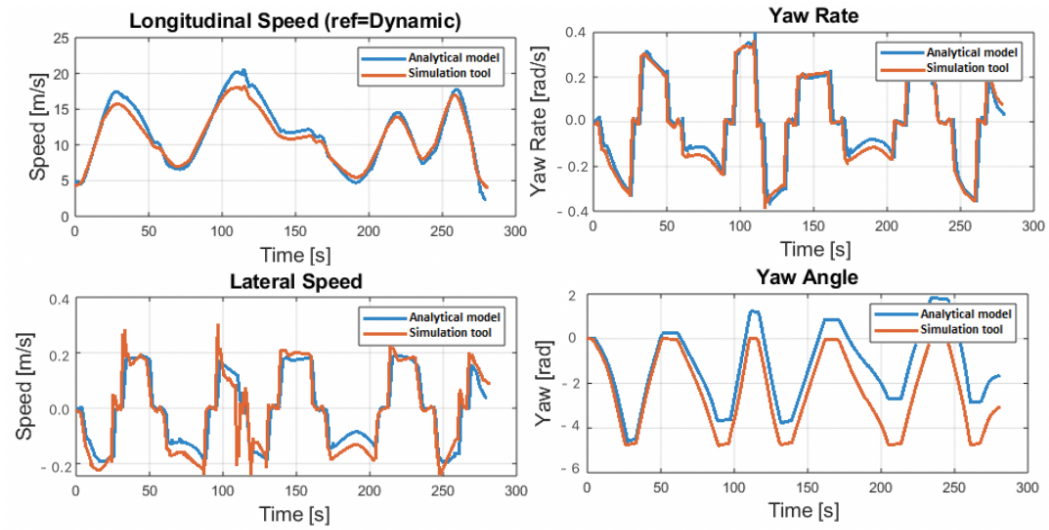

Figure 21. Dynamic speed results after sensitivity test.

As shown in Figure 22, even though the yaw angle implies the error percentage is still significant, the improved results allow for a forecast horizon of 66 s when an acceptable yaw error is less than 10%. Results may be satisfactory up to a speed of 60 km/h (urban speed profile); however, the lateral dynamic model can reproduce the mechanical behavior of a motorcycle in the presence of roll, slope, and bank angles with a maximum error of 10% on time around 1 min; this error represents an unacceptable energetic representation in the electric model. The lateral dynamic model's maximum speed values will be used as constraints in estimating behavior since their primary function is to ensure the driver's safety and comfort over the proposed speed profile. Because of its ability to provide an energy estimate that is both fast and precise enough for use in the control phases, the longitudinal model is chosen.

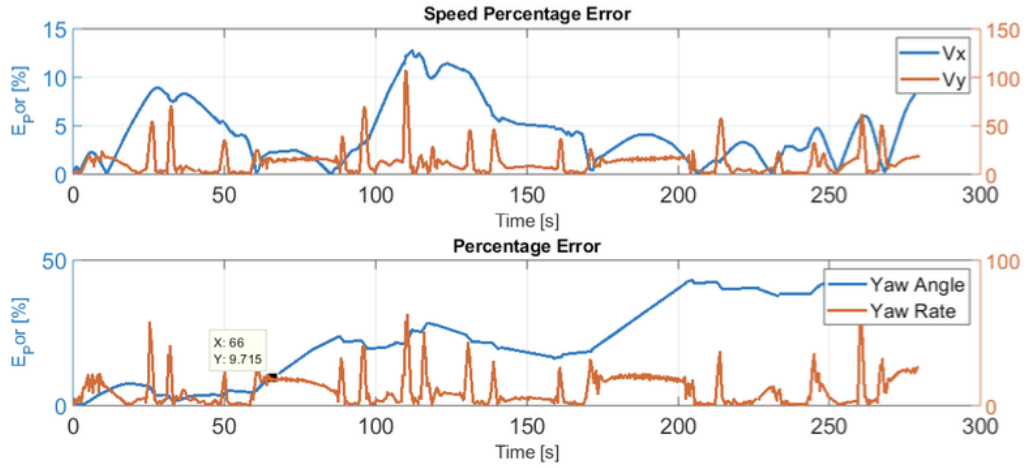

Figure 22. Dynamic speed profile results after sensitivity test (error percentage).

6. Test Results

This section covers the elements needed to determine the eco-driving strategy's operating torque and speed range. The purpose of the exam is to:

- Expected autonomy exploration and comparison with autonomy attained using speed and position state feedback.
- To contrast predicted autonomy with autonomy attained in a particular scenario with energy feedback.
- The effect of the velocity estimator on the control signal is investigated. Because the velocity estimator has a 28% possibility of misinterpreting, this inaccuracy generates an initial energy estimate error that the closed-loop controller must fix. To understand the controller capabilities appropriately, the estimation results must address the worst-case scenario.

The first test consists in running the same distance many times at different speed profiles with a specific Set on β_2 value to establish the energy consumption throughout the path. Then, β_2 is varied to assess its impact on all velocity profiles, sensor, and actuator errors. Additionally, β_2 is adjusted based on the maximum normalized energy usage (kW/km) for each WLTC category (class 6, class 3, class 2, and class 1). Each criterion assesses the maximum normalized energy usage based on a rural and urban trajectory. Figure 23 illustrates the relationship between β_2 and the normalized peak energy consumption (kW/km). In Figure 24 is presented the autonomy behavior of the test.

The estimated autonomy in the test bench findings is reduced from 30% in simulation to 20%. The energy coefficient exhibited similar behavior to that observed in the simulation but with notable changes in autonomy. While the speed profiles have equal autonomy with low β_2 values, the simulations demonstrate that the "Class 3" speed profile is the most battery-consuming. Furthermore, rural speed profiles are more likely to improve autonomy than urban speed profiles. Both variances are due to motor power and projected efficiency function. The speed range of the motor is limited. It results in a distinct behavior of the efficiency function, leading the stop times and lower speed trajectories to be more efficient than in a larger motor, even when the speed profiles are normalized to be coherent between both tests. At the same time, there are striking parallels. The ranges of autonomy estimation are still consistent across the two studies. Except for the "NREL Class 3" speed profile in its urban and rural approaches, the autonomy variation of β_2 from minimum to maximum is roughly 20% (in the simulation experiment, it was 30%). Because of the halted time in each speed profile, the autonomy augmentation recorded by the "Class 3" speed profile is more significant than 30% in both circumstances (simulation and test bench). The controller's primary function is to assure the trip distance required by the driver under various beginning conditions. For these reasons, it is important to investigate the dynamic

of energy estate and how β values can correct miscalculations caused by the speed profile estimator.

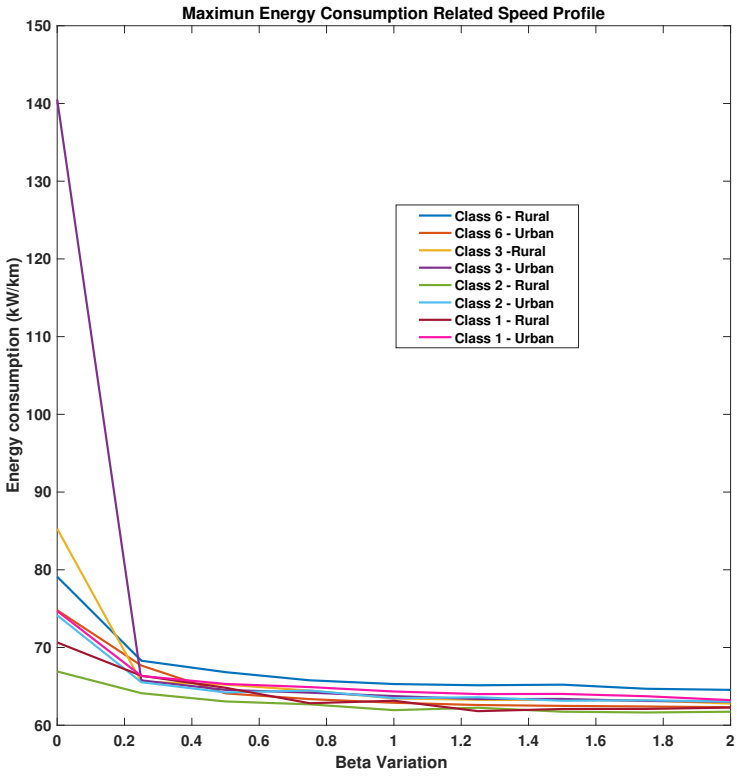

Figure 23. Energy coefficient along each speed profile.

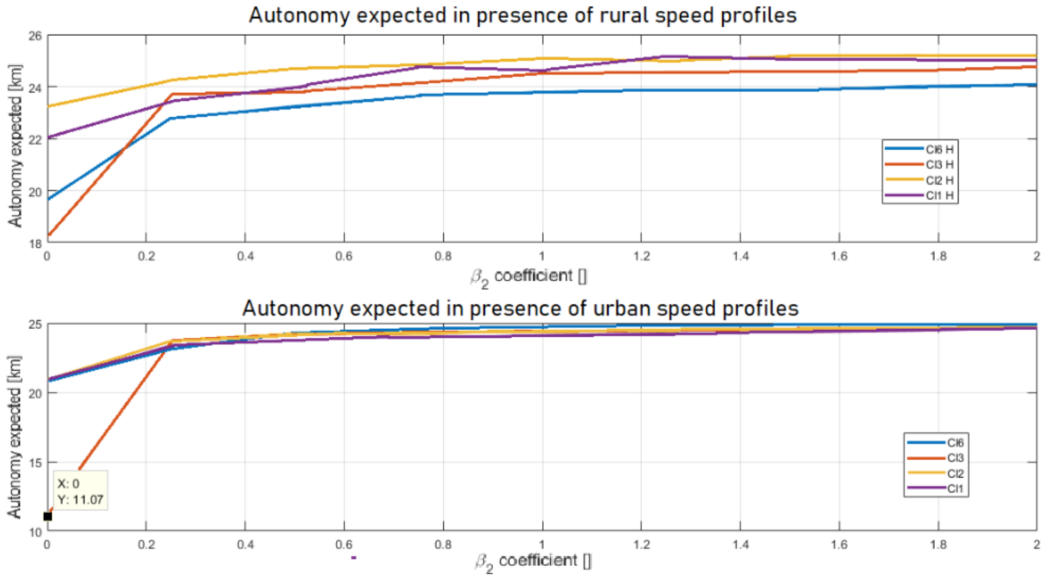

Figure 24. Autonomy comparison.

In the second test, the energy state is sent to the controller so that the energy coefficient can be fixed through the β_2 parameter. This value is dynamically varied from 0 to 5 $\beta_{2_{maxA}}$ without traffic restrictions and from 0 to 2 with traffic constraints $\beta_{2_{maxNA}}$. The test results are provided in Table 3.

Table 3. Closed-Loop distance error values.

Maximum $\beta_2 \rightarrow \beta_{2_{maxA}}$				
SOC [%]	Expected by Estimator [km]	Reference [km]	Computed [km]	Distance Error [%]
100	79.70	71.73	71.05	−0.95
50	39.84	35.86	35.48	−1.06
20	15.93	14.34	14.07	−1.92
Middle $\beta_2 \rightarrow \beta_{2_{maxNA}}$				
SOC [%]	Expected by Estimator [km]	Reference [km]	Computed [km]	Distance Error [%]
100	70.5	70.5	70.61	0.16
50	35.25	35.25	35.25	0.54
20	14.1	14.1	14.08	0.09
Minimum $\beta_2 \rightarrow \beta_{2_{min}}$				
SOC [%]	Expected by Estimator [km]	Reference [km]	Computed [km]	Distance Error [%]
100	60.7	60.7	64.07	5.49
50	30.36	30.36	32	5.4
20	12.1	12.14	12.24	0.8

As can be seen, distance error (difference between driver request and vehicle location) is always less than 5.5%. This indicator can improve if only cases in which the trip still needs to be completed are considered. These produce error decreases to approximately 2% in the absence of traffic conditions.

Under traffic conditions where β_2 cannot be rapidly saturated due to unplanned stops and a brief period where traffic is not restricted (the vehicle is stopped), distance error drops to a minimum of 0.6%, which means the eco-driving approach can guarantee 99.4% of the distance required by the driver under realistic traffic, weather, and road circumstances. This result shows an optimum speed profile with a correlation of approximately 0.87 with the driver-proposed initial speed profile. The speed profile provided by the NMPC can be seen in Figure 25. The maximum and minimum values are avoided in experimental findings and simulation, except for unplanned stops. The resulting speed profile is sensitive to speed changes proposed by the driver. It maintains a soft constraint over the speed values to ensure the safety and comfort of passengers and dynamically controls the intended energy consumption rate by integrating the speed constraint. All reported results do not account for estimated errors. It indicates that the speed profile calculation was accurate in every instance. The estimator's precision is 72%. The impact of this inaccuracy is examined in the following section.

This evaluation uses a variety of speeds and accelerations to try to guess how much energy will be needed to finish the trip, whether in a city or a rural setting. Appropriately approximating the speed profile (rural or urban) yields accurate estimates. The estimation error is 72% when the data is less than 120 s and 88% when it is 500 s. Then, from this concept, Figures 26 and 27 show two situations of correct estimation via the behavior of the signal $beta_2$ and its effect on the estimated range along the route. The anticipated speed profile utilized in instance A is "class 3 urban", with SOC in 100% for the start and 70.5 km of distance trip. The estimation is correct in this situation, but due to the inaccuracy produced by the amplitude of the disturbance relative to the velocity signal, β_2 must fix the energy parameter to demand the suitable energy required and reduce the distance error to 0.82%. However, in some circumstances, the perturbation magnitude is modest enough that the β_2 value does not need to be corrected. Figure 27 depicts an example of

this circumstance. The estimation and used velocity profile are equaled, except because the initial SOC is 20%, and the distance is 14.1 km. The distance inaccuracy in this situation is roughly 0.18 m.

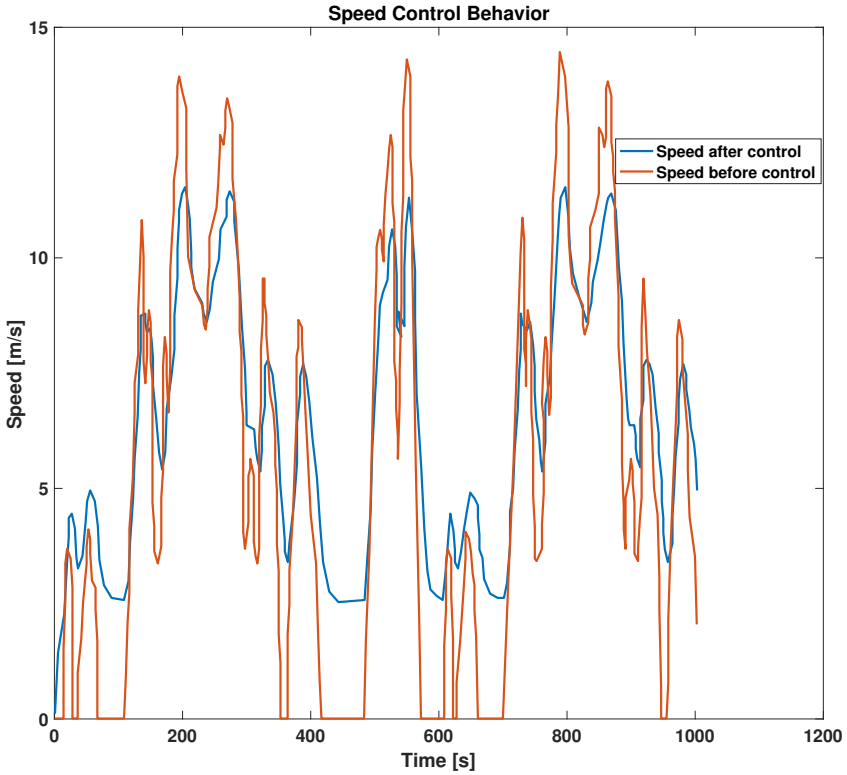

Figure 25. Effect of speed estimation.

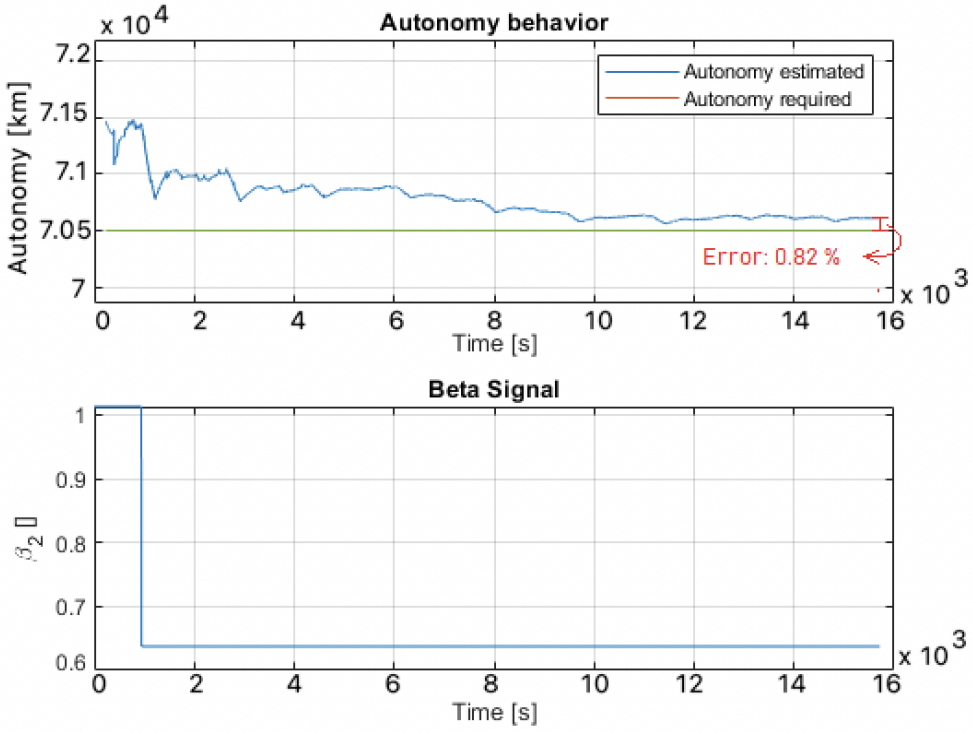

Figure 26. Case A, Good estimation.

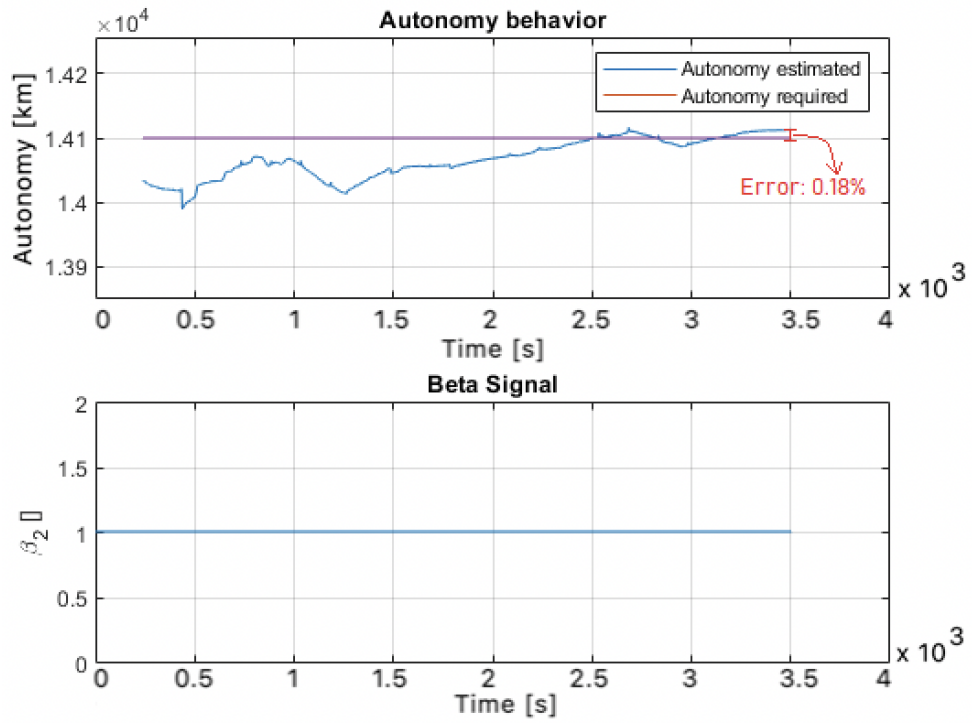

Figure 27. Case B, Good estimation.

Between proper and inaccurate categorization, a medium category will be designated (wrong estimation). An accurate velocity estimation seeks to decrease the distance error, but the random behavior of the disturbances accounts for a significant portion of the error compared to the speed data. The proportional energy controller can manage the energy coefficient inaccuracy with some time delays if the speed profile is incorrect, but the approach (rural or urban) is right. The outcomes of these cases are depicted in Figure 28. In this scenario, the starting SOC is 50% and is configured at 35.25 km for the trip. The inaccuracy induced by incorrect velocity profile estimation generates an inaccuracy corrected by the controller, but the control signal is sluggish due to the significant variation in sampling time. In those circumstances, though, the distance inaccuracy remains at approximately 1.3 percent. This final distance mistake is determined by the amount of distance traveled and the misunderstood speed profile.

A "completely erroneous estimation" is achieved when the urban/rural approach and velocity profile are misconstrued or the anticipated velocity profile has a high energy coefficient compared to the genuine one. As seen in Figure 29, the control signal saturates itself to minimize the energy coefficient error as much as possible. If the required distance is short, the inaccuracy can be as low as 4% if enough time is allowed. The inaccuracy is even reduced to 2.12%. (as in the presented example). In certain circumstances, the control signal climbs to the maximum speed variable limitations, resulting in a trip that behaves more like a driver-controlled experience than an autonomous experience.

Furthermore, the distance error is negative, indicating that the vehicle will not be able to complete the journey. The likelihood of encountering this circumstance within a measurable period of 120 s is approximately 20%. This reduces the possibility of completing the trip with a distance error of less than 1.5% from 98.4% to 78.4%. As a result, an additional estimating tool is used. When the difference between the predicted and observed energy coefficient is more than 10 W/m, the rural/urban approach estimates are replaced by the hypothetical rural/urban approach inferred from the road type used (highway, urban road, etc.). Using this approach, if the distance error is about 1.3 percent and the error is positive, it is considered "totally incorrect estimation", in addition to "bad estimation" (It means the trip is completed with the remaining energy in the battery).

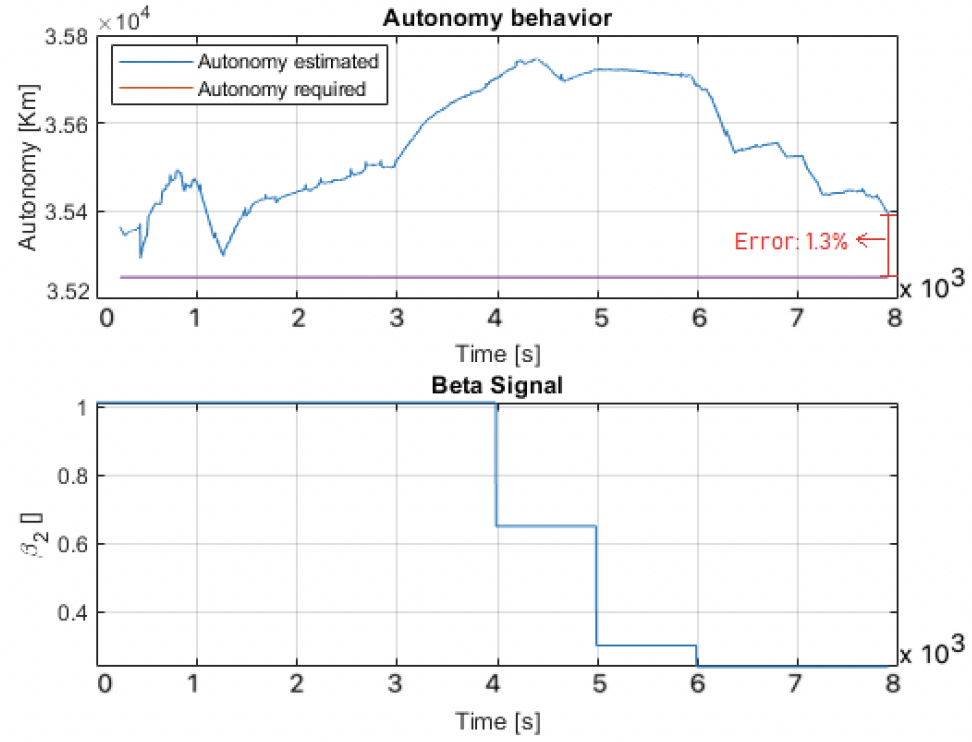

Figure 28. Correct urban/rural estimation.

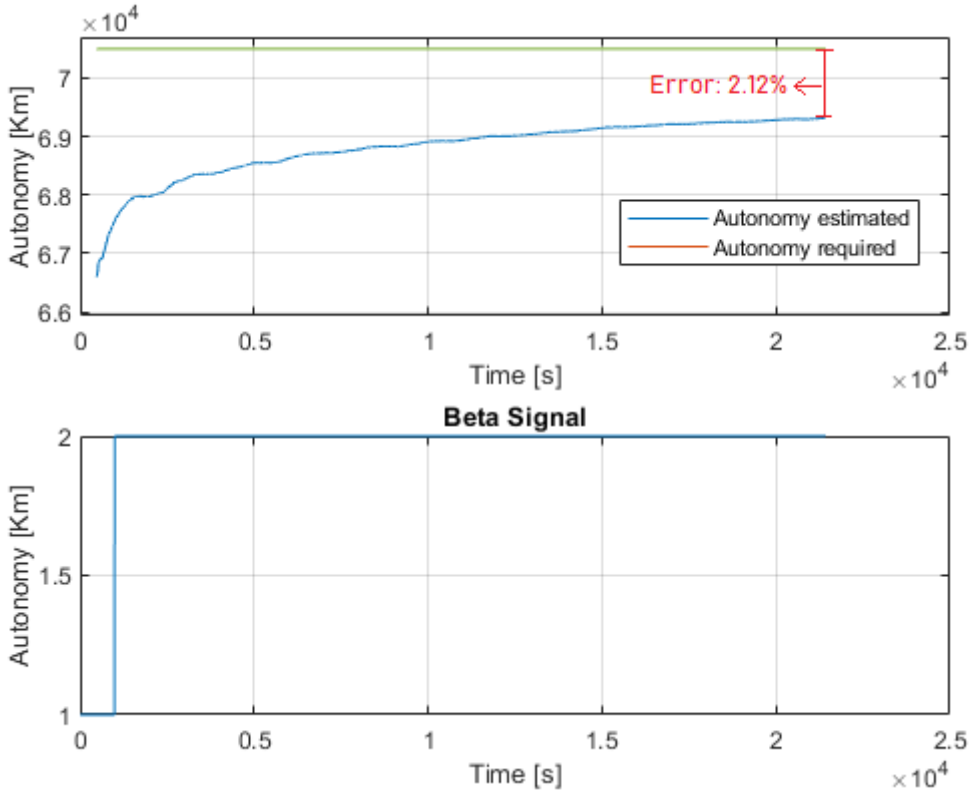

Figure 29. Bad speed profile estimation.

7. Conclusions

This article presented a practical energy-efficient non-linear model predictive for an electric two-wheeler vehicle with different driving profiles and driver preferences. In the proposal, the feedback loop allows energy computation and estimates the parameters in

the cost function of the problem. Moreover, it is shown how to implement the NMPC in a test bed with its specifications and the different test. The proposed method has been successful regarding the energy consumption of the vehicle. Indeed, the presented implementation concludes that the NMPC can be used under realistic conditions with specific configurations well adapted to real-time operation. Comparisons with simulations showed an excellent approach. Even if the speed profile estimator has 72% reliability, the supplemental information on the rural/urban component of the speed profile derived from historical data was enough to guarantee a 98% probability of finishing the trip with various initial SOC or driving behaviors. The gap between the absolute needed and the final required distance was less than 1.5 percent. The distance error is positive in 98% of the cases, which indicates that the distance traveled is always more significant than the amount required by the driver. Finally, the tighter speed profile restrictions allow for a 20% increase in autonomy.

Future research could compare and improve new speed profile estimators to mitigate this effect. Lastly, estimating energy use increases autonomy by about 20%, even when the estimated speed profile keeps a 68% correlation with the driver's most demanding speed profile. The eco-driving technique suggested and validated in this work effectively reduces the energy requirements for transportation. It is a tool for increasing the presence of electric vehicles in the transportation sector due to the driver's confidence in the vehicle's autonomy capacity and the reduction in energy needs.

Author Contributions: Methodology Y.B., T.A., J.S.R. and D.P.; Implementation Y.B.; validation, Y.B., T.A., J.S.R. and D.P.; formal analysis, Y.B., T.A., J.S.R. and D.P.; research, Y.B., T.A., J.S.R. and D.P.; physical resources, Y.B., T.A., C.L., N.R., M.B. and F.R.; writing—original draft preparation, Y.B., T.A., J.S.R. and D.P.; writing—review and editing, C.L., N.R. and M.B., F.R., Y.B., T.A., J.S.R. and D.P.; design, Y.B., J.S.R., D.P. and T.A.; supervision, C.L., N.R., M.B., F.R., T.A. and D.P.; project administration, C.L., N.R., M.B., F.R., T.A. and D.P.; funding acquisition, T.A. and D.P. All authors have read and agreed to the published version of the manuscript.

Funding: This research was funded by: Minciencias, ECOSNORD project 890-2019, and grant number 779 of 2017 by Boyaca government.

Institutional Review Board Statement: Not applicable.

Informed Consent Statement: Not applicable.

Data Availability Statement: Not applicable.

Acknowledgments: Authors want to thank Minciencias, ECOSNORD for the sponsorship to the project "Control asistido para la conducción de una motocicleta eléctrica orientado a la eficiencia energética" with contract 890-2019, and Boyacá government grant number 779 of 2017.

Conflicts of Interest: The authors declare no conflict of interest.

Abbreviations

ADAS	Advance Driver Assistance System
BLDC	Brushless DC
EV	Electric Vehicles
FOC	Feld-Oriented Control
GUI	User Graphic Interface
MPC	Model Predictive Controller
NMPC	Nonlinear Model Predictive Controller
NREL	National Renewable Energy Laboratory Drive Cycle
PI	Proportional–Integral
SOC	State of Charge
WLTC	Worldwide harmonized Light-duty vehicles Test Cycles

Nomenclature

$\ddot{x}$	Acceleration
F_{aer_x}	Aerodynamic Force in X-axis
ρ	Air Density
α_{air}	Angle Between Air and Vehicle Direction
β	Bank Angle
N_c	Control Horizon
$\dot{x}_1$	Distance
C_d	Drag Coefficient
R_{wf}	Effective Radius of Rear Wheel
EVs	Electric Vehicles
E	Energy
ϵ_{e_c}	Energy necessary to end the trip
t_f	Final Time
A_f	Front Area
g	Gravity
t_0	Initial Time
m	Mass
T_{max}	Maximum Torque
T_{min}	Minimum Torque
$E_{ff}(X_2, T)$	Motor Efficiency Abstraction
F_z	Normal Force
β_{11}	Cost Function Normalized coeff
β_{13}	Cost Function Normalized coeff
β_{12}	Cost Function Normalized coeff
N_p	Prediction Horizon
$\mu_{0,1,2}$	Road Parameters
$\mu_{1,2}$	Road Parameters
F_{roll}	Roll Resistance
s	Seconds
θ_s	Slope
$\dot{x}$	Speed
t	Time
t_s	Time Period (1000 s)
T	Torque
TotEne	Total Energy
d(t)	Travel Distance
F_l	Uncontrolled Torque Inputs (losses)
$\dot{x}_3$	Vehicle energy
$\dot{x}_2$	Vehicle Speed
F_w	Weight
V_{wind}	Wind Speed

References

1. Bugaje, A.; Ehrenwirth, M.; Trinkl, C.; Zörner, W. Electric two-wheeler vehicle integration into rural off-grid photovoltaic system in Kenya. *Energies* **2021**, *14*, 7956. [CrossRef]
2. Xue, Q.; Wang, K.; Lu, J.J.; Liu, Y. Rapid driving style recognition in car-following using machine learning and vehicle trajectory data. *J. Adv. Transp.* **2019**, *2019*, 9085238. [CrossRef]
3. Musa, A.; Pipicelli, M.; Spano, M.; Tufano, F.; De Nola, F.; Di Blasio, G.; Gimelli, A.; Misul, D.A.; Toscano, G. A review of model predictive controls applied to advanced driver-assistance systems. *Energies* **2021**, *14*, 7974. [CrossRef]
4. Gao, G.; Wang, Z.; Liu, X.; Li, Q.; Wang, W.; Zhang, J. Travel behavior analysis using 2016 Qingdao's household traffic surveys and Baidu electric map API data. *J. Adv. Transp.* **2019**, *2019*, 6383097. [CrossRef]
5. Rahimi-Eichi, H.; Chow, M.Y. Big-data framework for electric vehicle range estim. In Proceedings of the IECON 2014-40th Annual Conference of the IEEE Industrial Electronics Society, Dallas, TX, USA, 29 October–1 November 2014; pp. 5628–5634.
6. Zhang, Y.; Wang, W.; Kobayashi, Y.; Shirai, K. Remaining driving range estimation of electric vehicle. In Proceedings of the 2012 IEEE International Electric Vehicle Conference, Greenville, CA, USA, 4–8 March 2012; pp. 1–7.
7. Lin, X.; Görges, D.; Liu, S. Eco-driving assistance system for electric vehicles based on speed profile optimization. In Proceedings of the 2014 IEEE Conference on Control Applications (CCA), Juan Les Antibes, France, 8–10 October 2014; pp. 629–634.

8. Kato, H.; Ando, R.; Kondo, Y.; Suzuki, T.; Matsuhashi, K.; Kobayashi, S. Comparative measurements of the eco-driving effect between electric and internal combustion engine vehicles. In Proceedings of the 2013 World Electric Vehicle Symposium and Exhibition (EVS27), Barcelona, Spain, 17–20 November 2013; pp. 1–5.
9. Farzaneh, A.; Farjah, E. a novel smart energy management system in pure electric motorcycle using COA. *IEEE Trans. Intell. Veh.* **2019**, *4*, 600–608. [CrossRef]
10. Koch, A.; Teichert, O.; Kalt, S.; Ongel, A.; Lienkamp, M. Powertrain Optimization for Electric Buses under Optimal Energy-Efficient Driving. *Energies* **2020**, *13*, 6451. [CrossRef]
11. Chen, C.; Zhao, X.; Yao, Y.; Zhang, Y.; Rong, J.; Liu, X. Driver's eco-driving behavior evaluation modeling based on driving events. *J. Adv. Transp.* **2018**, *2018*, 1–12. [CrossRef]
12. Hieu, L.T.; Khoa, N.X.; Lim, O. An Investigation on the Effects of Input Parameters on the Dynamic and Electric Consumption of Electric Motorcycles. *Sustainability* **2021**, *13*, 7285. [CrossRef]
13. Benotsmane, R.; Vásárhelyi, J. Towards Optimization of Energy Consumption of Tello Quadrotor with MPC Model Implementation. *Energies* **2022**, *15*, 9207. [CrossRef]
14. Bello, Y.; Azib, T.; Larouci, C.; Boukhnifer, M.; Rizoug, N.; Patino, D.; Ruiz, F. Eco-Driving Optimal Controller for Autonomy Tracking of Two-Wheel Electric Vehicles. *J. Adv. Transp.* **2020**, *2020*, 1–15. [CrossRef]
15. Kamal, E.; Adouane, L. Optimized EMS and a Comparative Study of Hybrid Hydrogen Fuel Cell/Battery Vehicles. *Energies* **2022**, *15*, 738. [CrossRef]
16. Zhang, X.; Mi, C. *Vehicle Power Management: Modeling, Control and Optimization*; Springer Science & Business Media: Berlin/Heidelberg, Germany, 2011.
17. Rajamani, R. *Vehicle Dynamics and Control*; Springer Science & Business Media: Berlin/Heidelberg, Germany, 2011.
18. Bello, Y.; Azib, T.; Larouci, C.; Boukhnifer, M.; Rizoug, N.; Patino, D.; Ruiz, F. Two wheels electric vehicle modelling: Parameters sensitivity analysis. In Proceedings of the 2019 6th International Conference on Control, Decision and Information Technologies (CoDIT), Paris, France, 23–26 April 2019; pp. 279–284.
19. Jazar, R.N. *Vehicle Dynamics*; Springer: Berlin/Heidelberg, Germany, 2008; Volume 1.
20. Cossalter, V.; Lot, R.; Massaro, M. Motorcycle dynamics. *Modelling, Simulation and Control of Two-Wheeled Vehicles*; Wiley: Hoboken, NJ, USA, 2014; pp. 1–42.
21. Sun, Z.; Wen, Z.; Zhao, X.; Yang, Y.; Li, S. Real-world driving cycles adaptability of electric vehicles. *World Electr. Veh. J.* **2020**, *11*, 19. [CrossRef]
22. Jape, S.R.; Thosar, A. Comparison of electric motors for electric vehicle application. *Int. J. Res. Eng. Technol.* **2017**, *6*, 12–17. [CrossRef]
23. Atallah, K.; Howe, D.; Mellor, P.H.; Stone, D.A. Rotor loss in permanent-magnet brushless AC machines. *IEEE Trans. Ind. Appl.* **2000**, *36*, 1612–1618.
24. Bianchi, N.; Bolognani, S.; Frare, P. Design criteria for high-efficiency SPM synchronous motors. *IEEE Trans. Energy Convers.* **2006**, *21*, 396–404. [CrossRef]
25. Song, L.; Li, Z.; Cui, Z.; Yang, G. Efficiency map calculation for surface-mounted permanent-magnet in-wheel motor based on design parameters and control strategy. In Proceedings of the 2014 IEEE Conference and Expo Transportation Electrification Asia-Pacific (ITEC Asia-Pacific), Beijing, China, 31 August–3 September 2014; pp. 1–6.
26. Fasil, M.; Mijatovic, N.; Jensen, B.B.; Holboll, J. Nonlinear dynamic model of PMBLDC motor considering core losses. *IEEE Trans. Ind. Electron.* **2017**, *64*, 9282–9290. [CrossRef]
27. Neacă, M.I.; Neacă, A.M. Determination of the power loss in inverters which supplies a BLDC motor. In Proceedings of the 2016 International Symposium on Fundamentals of Electrical Engineering (ISFEE), Bucharest, Romania, 30 June–2 July 2016; pp. 1–6.
28. Rong, Y.; Yang, W.; Wang, H.; Qi, H. SOC estimation of electric vehicle based on the establishment of battery management system. In Proceedings of the 2014 IEEE Conference and Expo Transportation Electrification Asia-Pacific (ITEC Asia-Pacific), Beijing, China, 31 August–3 September 2014; pp. 1–5.
29. Lee, K.Y.; Lai, Y.S. A novel magnetic-less bi-directional dc-dc converter. In Proceedings of the 30th Annual Conf. of IEEE Industrial Electronics Society IECON 2004, Busan, Republic of Korea, 2–6 November 2004; Volume 2, pp. 1014–1017.
30. Cristhian Yesid, B.C. Eco-Driving Planification Profile for Electric Motorcycles. Ph.D. Thesis, Paris-saclay, Pontficia Universidad Javeriana, Bogota, Colombia, 2020.
31. Bello, Y.; Azib, T.; Larouci, C.; Boukhnifer, M.; Rizoug, N.; Patino, D.; Ruiz, F. Motor efficiency modeling towards energy optimization for two-wheel electric vehicle. *Energy Effic.* **2022**, *15*, 1–14. [CrossRef]